Monthly Notices of the ROYAL ASTRONOMICAL SOCIETY

MNRAS **497,** 2201–2212 (2020) doi:10.1093/mnras/staa2089
Advance Access publication 2020 July 17

Binary fraction indicators in resolved stellar populations and supernova-type ratios

E. R. Stanway [1]★ J. J. Eldridge [2] and A. A. Chrimes [1]

[1] *Department of Physics, University of Warwick, Gibbet Hill Road, Coventry CV4 7AL, UK*
[2] *Department of Physics, University of Auckland, Private Bag 92019, Auckland, New Zealand*

Accepted 2020 July 13. Received 2020 July 13; in original form 2020 June 15

ABSTRACT

The binary fraction of a stellar population can have pronounced effects on its properties, and, in particular, the number counts of different massive star types, and the relative subtype rates of the supernovae (SNe) that end their lives. Here we use binary population synthesis models with a binary fraction that varies with initial mass to test the effects on resolved stellar pops and SNe, and ask whether these can constrain the poorly-known binary fraction in different mass and metallicity regimes. We show that Wolf–Rayet (WR) star subtype ratios are valuable binary diagnostics, but require large samples to distinguish by models. Uncertainties in which stellar models would be spectroscopically classified as WR stars are explored. The ratio of thermonuclear, stripped-envelope, and other core-collapse SNe may prove a more accessible test and upcoming surveys will be sufficient to constrain both the high- and low-mass binary fraction in the $z < 1$ galaxy population.

Key words: methods: numerical – binaries: general – stars: evolution – galaxies: stellar content.

1 INTRODUCTION

Stellar population synthesis models provide a framework through which observational data of stellar clusters, galaxies, and galaxy populations can be interpreted (Tinsley & Gunn 1976). Identifying the properties of the observed population relies on matching the data to predictions determined by the age, mass, metallicity, and other properties of the best-fitting model. Those predictions are sensitive to the assumed evolution of individual stars included in the synthesis model, which, in turn, depends on assumptions including the fraction of stars affected by binary evolution pathways.

While the majority of stellar population and spectral synthesis models currently in use neglect the role of stellar multiplicity (e.g. Bruzual & Charlot 2003; Le Borgne et al. 2004; Maraston 2005), there is an increasing recognition that its effects are important, particularly when interpreting young and distant stellar populations, or in determining the rates of transient objects (e.g. Vrancken et al. 1991; Tutukov, Yungelson & Iben 1992; De Donder & Vanbeveren 1998; Vanbeveren et al. 1998; Zhang et al. 2013; Stanway et al. 2014; Eldridge & Stanway 2016; Ma et al. 2016; Stanway, Eldridge & Becker 2016; Steidel et al. 2016, 2018; Wilkins et al. 2016; Eldridge, Stanway & Tang 2019; Chrimes, Stanway & Eldridge 2020; Götberg et al. 2020; Zapartas et al. 2020). The fraction of massive stars affected by a binary companion during their evolution is clearly substantial, and cannot be entirely neglected (Sana et al. 2012, 2013). None the less, implementing binary evolution pathways is both technically challenging and involves introducing additional assumptions for the binary fraction, and the distribution of initial binary parameters in the population, as well as the initial mass function (IMF). Constraints on these parameters have improved significantly in recent years (Moe & Di Stefano 2017; Moe, Kratter & Badenes 2019; Traven et al. 2020), but remain poor at low metallicities and outside the local Universe.

In Stanway & Eldridge (2019), we began a programme to explore the impact of these uncertainties on stellar population predictions, by varying the IMF parameters assumed by the Binary Population and Spectral Synthesis (BPASS; Eldridge et al. 2017, hereafter E17) model framework, while keeping the binary parameters fixed. In Stanway et al. (2020, hereafter S20), we instead explored the impact of stellar binary population parameter uncertainties on the integrated light of stellar populations for a fixed IMF. In that work, we considered both observational uncertainties on the binary parameters in the current v2.2 of BPASS, which are based on the analysis of Moe & Di Stefano (2017, hereafter MS17), and an extended grid of models in which the binary fraction as a function of mass is varied by an arbitrary amount.

In parallel, recent work by Dorn-Wallenstein & Levesque (2018, 2020) has explored the effect of both binary fraction and rotation on predictions for resolved stellar populations, using a custom set of models in which stars of all masses are assumed to share a common binary fraction. They identified the ratio of certain massive stellar types, and, in particular, the ratio of stripped-envelope, strong-wind, helium-atmosphere Wolf–Rayet (WR) stars to red supergiant (RSG) stars, as being sensitive to the binary fraction (and indeed rotational mixing) assumed.

Here we explore the impact of a mass-dependent binary fraction on both stellar-type ratios and supernova (SN)-type ratios using a grid of models with a wide range of possible initial mass-dependent binary fractions and metallicities. We explore whether binary fractions might be recovered from observations of resolved stellar populations in the local Universe, or of bright transients

★ E-mail: e.r.stanway@warwick.ac.uk

at cosmological distances. We also explore the impact on these interpretations of recent proposals that the minimum luminosity of WR stars identified spectroscopically may show a strong metallicity dependence.

The structure of this paper is as follows: In Section 2, we introduce the model grid used here and discuss the alternate definitions of WR stars. In Section 3.1, we present the predictions of our models for continuously star-forming populations as a function of metallicity. In Section 3.2, we consider the binary fraction influence on SN rates and the ratio between SN types, assuming appropriate redshift histories for both star formation and its metallicity distribution. We evaluate the impact of WR definition and of binary fraction on these predictions, and consider whether upcoming projects will enable binary fraction to be evaluated observationally in future, in Section 4. Finally, we summarize our main conclusions in Section 5.

2 METHOD

2.1 Standard models

All models presented here are based on the BPASS stellar population synthesis models (Eldridge & Stanway 2009, 2012; Stanway et al. 2016; E17), specifically their v2.2.1 implementation (Stanway & Eldridge 2018). This framework generates an evolving simple (i.e. coeval) stellar population in which the initial stellar masses are distributed according to a broken power law, and the binary fraction, initial period distribution, and initial mass ratio distribution of stars are based on the distributions determined by MS17. These were initially determined empirically for stars in five mass ranges and four initial period bins, and are interpolated on to the BPASS mass and period grid. Here we keep the IMF, initial period distribution, and mass ratio distributions fixed in line with the BPASS v2.2 default, but vary the binary fraction with the logarithm of the mass of the primary star.

As in S20, where the unresolved stellar populations derived from the same models are discussed, we define two sets of variant models. In set 1, the high-mass binary star fraction (above 20 $M_\odot$) is fixed at unity and the low-mass binary fraction is permitted to vary from about 40 per cent at Solar mass up to unity. In set 2, the Solar mass binary star fraction is held fixed at about 40 per cent, but the high-mass binary fraction is permitted to vary from its current estimate (near unity) down to 40 per cent. These sets of varying binary fractions are defined in Fig. 1 and discussed in detail in S20.

We note that this approach differs from and is complementary to that of Dorn-Wallenstein & Levesque (2018, 2020) in which stars of all masses are deemed to share a common binary fraction, in conflict with the observed distributions in the local Universe. Since those papers addressed the relative numbers of massive stars, derived from a relatively narrow range of initial masses in young populations, their assumption of a constant binary fraction over that mass range is likely reasonable. However, we expect the dependence on initial mass to affect any comparison with populations arising from lower mass stars, for example, in the ratios of different SN types as a function of metallicity or age, or their cosmic evolution (as discussed in Section 3.2).

The models presented here do not vary the distribution of initial binary separation and mass ratio due to computational constraints, but focus on the total binary fraction as a function of primary star mass. The effects of varying these parameters independently was explored for unresolved stellar populations by S20, and it is clear that the current observational constraints on separation and mass ratio permit a large range of possible models. In the context of the work on resolved populations in this paper, the key question to be addressed is whether binary interactions alter the evolution of a system, thus changing its stellar type or SN type at death. A system is more likely to interact if the stars begin their life in a close binary or if the mass ratio between primary and companion is near unity. Thus, an increase in the total binary fraction has a similar effect to biasing the initial period distribution towards shorter periods, or to biasing the mass ratio towards twin systems. The default BPASS prescription for these is fixed based on observational constraints derived as a function of stellar mass by MS17, and, for massive stars, already include a bias towards twin systems and short periods. Thus, varying the overall binary fraction captures the majority of the behaviour for massive stars. For lower mass (e.g. Solar-type) stars, the distributions are broader and the observational constraints weaker, and so models in set 1 will be degenerate with models with larger mean separations or smaller mass ratios.

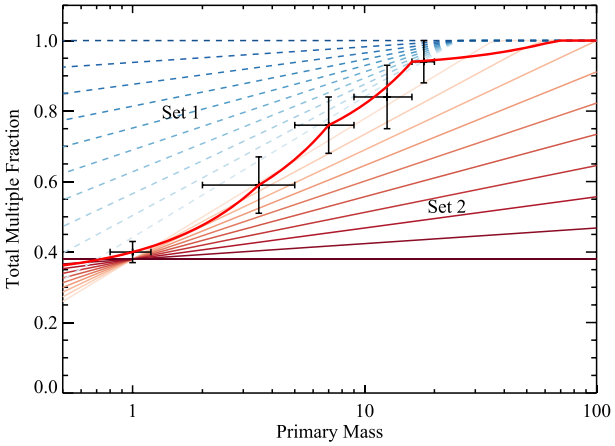

Figure 1. Multiple fractions tested in an experimental grid to examine possible observable signatures for binary populations. Each line indicates a model binary fraction distribution that either raises the binary fraction at low stellar mass (set 1, dashed lines) or lowers it at high mass (set 2, solid lines). Data points are drawn from MS17 and the thick red line indicates the fiducial model applied in BPASS v2.2.C

For each variant binary fraction versus mass distribution function, we calculate time-evolving stellar number counts for populations with an initial total stellar mass of 10^6 $M_\odot$ at 13 metallicities and 42 age steps, spaced logarithmically such that $\log(\text{age/years}) = 6.0 + i \times \Delta(\text{age})$ ($i = 0$–41) and the increment $\Delta(\text{age}) = 0.1$. For each of these age steps, we assign each stellar model a type by luminosity, temperature, and surface composition.

Similarly, we assign a type to each SN identified based on the state of its progenitor at the end of its evolution. These classifications are described in E17. Briefly, a star is considered to undergo a core-collapse SN if it has undergone core carbon burning and has a CO-core mass >1.38 $M_\odot$ at the end of its life. Its type is then determined by the chemical composition of the surface layers which will be ejected, and the remnant (if any) determined from the core mass after accounting for the SN energy injection. The survival or disruption of the binary is determined probabilistically, given an assumed kick distribution. For stars with insufficient mass to undergo core collapse, the end state is deemed to be a white dwarf with the mass of the progenitor star's helium core at the end of its life. Binary systems that survive to this point can show an increase in the white dwarf mass through mass transfer from a companion, or a merger of double white dwarfs through angular momentum loss due to gravitational wave radiation. Where either of these pathways result in a white dwarf with

a total mass exceeding the Chandrasekhar limit, a thermonuclear, Type Ia SN (SN Ia) is deemed to occur. The rates and delay-time distributions of such explosive transients, as modelled in BPASS, are discussed in detail in Eldridge et al. (2019) and are shown to be consistent with observational constraints.

2.2 WR definition

In the standard models described above, we have used the WR definitions laid out in E17 in which stars are identified as WR based primarily on their surface compositions. Stars are assumed to be identifiable as strong wind-driving, WR stars, rather than lower mass helium stars, if they have a luminosity exceeding $\log(L/L_{\odot}) > 4.9$.

Recent work (Shenar et al. 2020) has argued on both observational and theoretical grounds that this simple constraint is insufficient. Instead, the luminosity constraint above which a star shows the spectral features classically identified as a WR may be metallicity dependent, scaling as $L^{\rm WR}_{\rm spec} \propto Z^{-1}$. Stars below this threshold would show a blue, stripped star spectrum, but produce narrow-line emission, rather than the strongly line-broadened emission associated with classical WRs.

To evaluate the impact of this proposal on the predicted number counts of stars by type, we recalculate the classification of stars in our models based on the relationship

$$\log_{10}\left(L^{\rm WR}_{\rm spec}\right) = 4.9 - \log_{10}(Z/0.014).$$

Only stars above this luminosity threshold are classified as WR. These models are shown on figures with dotted lines, where appropriate. We do not expect this change to affect SN rates, since these are determined by the structure and composition of the progenitor star, which is only weakly related to its stellar classification (e.g. Eldridge et al. 2018).

3 RESULTS

3.1 Trends with metallicity

3.1.1 Resolved stellar populations

The metallicity of stars affects their wind strengths, radii, surface gravity, and hence probability of undergoing binary interactions while on the main sequence or giant branch. Such interactions can lead to surface hydrogen stripping, rejuvenation, and other processes, which will change the classification of the stellar model. As a result, we expect (and observe) the ratio of different stellar types to depend on both binary fraction and metallicity.

We calculate trends in stellar-type number counts with metallicity for star-forming stellar populations. In each case, we assume that the composite stellar population (CSP) has been forming stars at a constant rate of 1 $M_{\odot}$ yr^{-1} for 100 Myr, such that the number counts of most stellar types have stabilized, with the rate of stellar birth balanced by the rate of stellar death for massive stars. The long-lived low-mass stellar population will continue to build up to much later ages, so we focus on the relatively massive stars that may be resolvable as individual stars beyond our immediate environs, and, in particular, on the WR population of stripped-atmosphere stars.

In Fig. 2, we show the dependence of the WR to O-star ratio in such a population on metallicity and binary fraction. Unsurprisingly, this ratio shows effectively no sensitivity to the binary fraction at low masses, with the models in set 1 indistinguishable at Solar metallicity. In contrast, the ratio is moderately dependent on the high-mass binary fraction for our standard WR definition. Number count ratios yielded by the revised Shenar et al. (2020) definition for WR stars show less

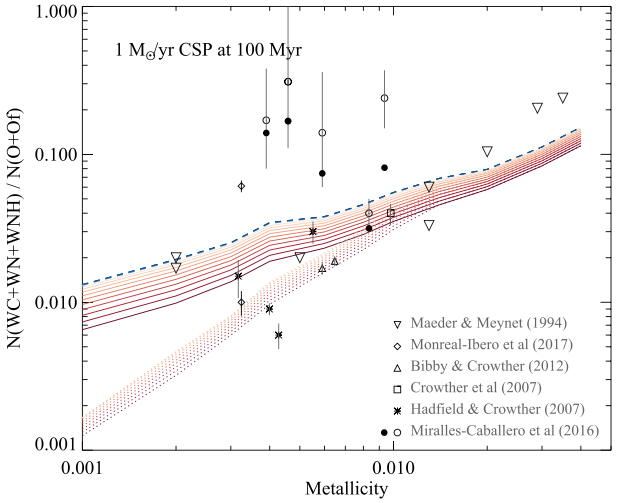

Figure 2. WR (WN + WC + WNH) to O-star (O + Of, $\log(L/L_{\odot}) > 4.9$) ratio, as a function of metallicity and a range of binary fractions. Models are as colour coded in Fig 1. Solid lines indicate a WR definition cut at $\log(L/L_{\odot}) > 4.9$, and dotted lines show a metallicity-dependent luminosity limit as discussed in Section 2.2. Data points are from the references labelled (Maeder & Meynet 1994; Crowther et al. 2007; Hadfield & Crowther 2007; Bibby & Crowther 2012; Miralles-Caballero et al. 2016; Monreal-Ibero et al. 2017). Filled symbols for Miralles-Caballero et al. (2016) indicate corrected values, as discussed in Section 4.1.

dependence on binary fraction, but a stronger metallicity dependence than those using a uniform luminosity definition.

For context, we also show a compilation of observational data points reported for this ratio (Maeder & Meynet 1994; Crowther et al. 2007; Hadfield & Crowther 2007; Bibby & Crowther 2012; Miralles-Caballero et al. 2016). In each case, we use the values reported by the original authors without modification. Where authors give metallicity in the form of 12 + log(O/H), we assume $Z = 0.020$ corresponds to 12 + log(O/H) = 8.93, as appropriate for BPASS stellar evolution models (E17; Xiao, Stanway & Eldridge 2018). We note that this observational data set is likely highly incomplete due to the difficulty of resolving large samples of massive stars, determining their metallicity and classifying them reliably, and we discuss this further in Section 4.1. As a result of these uncertainties, the observational data show a large scatter and it is difficult to draw firm conclusions from the data. None the less, the models demonstrate that precision on the WR fraction significantly better than 1 per cent is needed to distinguish between binary fraction models at metallicities near Solar, where the ratio ranges from 0.078 at a massive star binary fraction of unity to 0.058 at a fraction of 40 per cent.

A similar dependence on metallicity in seen in the WR subtype ratios shown in Fig 3. The fraction of carbon-rich WC stars in the population (relative to nitrogen-rich WN stars and partially stripped WNH stars) declines sharply with either decreasing metallicity or increasing binary fraction when a uniform luminosity cut for WR stars is used. Introducing a metallicity dependence to the WR luminosity threshold has the effect of strongly reducing the dependence on both metallicity and binary fraction in this ratio. For comparison, we show number counts for Galactic and Magellanic WR stars spanning a range of metallicities including the recent compilation from Rosslowe & Crowther (2015). While the uncertainties on these measurements are still very large, they also appear to disfavour the revised Shenar et al. (2020) WR star definition.

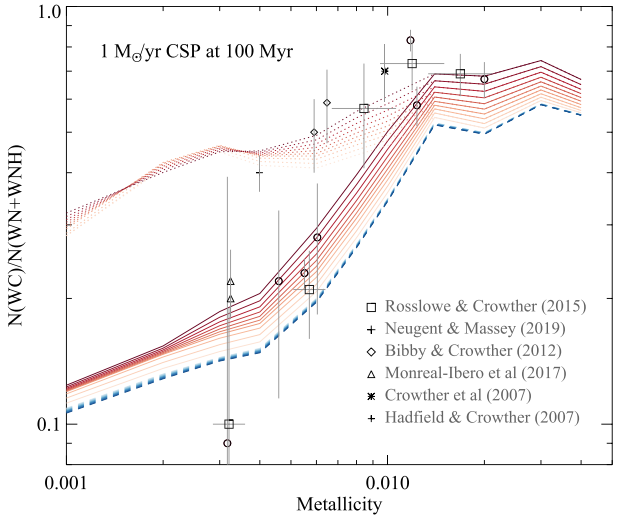

Figure 3. WR WN to WC ratio as a function of metallicity for binary fractions as colour coded in Fig 1. Dotted lines show the results for the revised WR definition. Data points are drawn from the literature (Crowther et al. 2007; Hadfield & Crowther 2007; Bibby & Crowther 2012; Rosslowe & Crowther 2015; Monreal-Ibero et al. 2017; Neugent & Massey 2019).

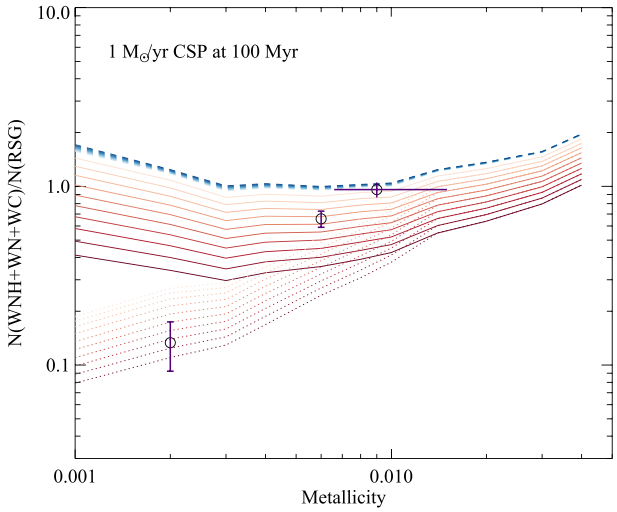

Figure 4. WR (WN + WC) to RSG (K + M, $\log(L/L_{\odot}) > 4.9$) ratio as a function of metallicity for binary fractions as colour coded in Fig 1. Dotted lines show the ratio for the revised WR luminosity limit. Data points are drawn from the literature (Massey & Olsen 2003; Massey et al. 2016; Neugent et al. 2018).

Another observation that has been suggested as a sensitive probe of massive star populations (e.g. Maeder, Lequeux & Azzopardi 1980; Massey, Neugent & Smart 2016; Dorn-Wallenstein & Levesque 2018; Neugent & Massey 2019) is the WR to RSG (defined in our models as K- or M-type stars with $\log(L/L_{\odot}) > 4.9$) ratio. We show the metallicty dependence of this ratio in our models in Fig. 4. Interestingly, and unlike the previous two ratios considered, this quantity is only mildly dependent on metallicity when using our standard WR definition, but very strongly dependent on massive star binary fraction (as also noted by Dorn-Wallenstein & Levesque 2018). This is a useful trait: The precise metallicity of stellar populations is often difficult to determine, particularly for more distant objects. Given the Shenar et al. (2020) WR definition, the

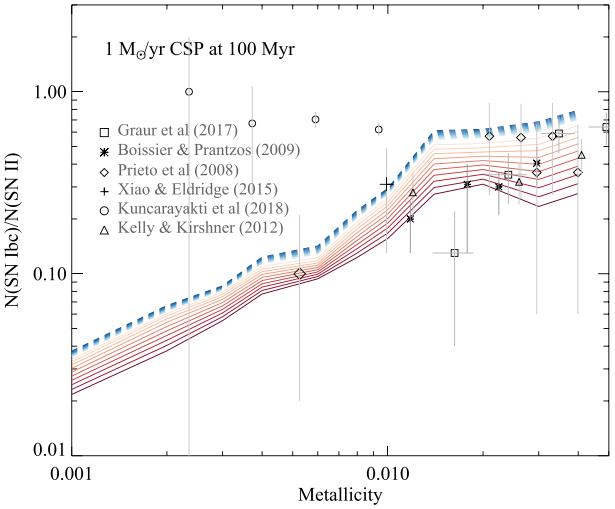

Figure 5. SN II to SN Ib/c ratio as a function of metallicity for binary fractions as colour coded in Fig 1. Metallicity differences or uncertainties swamp binary fraction ones. For comparison, we show a compilation of data from the literature with representative uncertainties (Prieto, Stanek & Beacom 2008; Boissier & Prantzos 2009; Kelly & Kirshner 2012; Xiao & Eldridge 2015; Graur et al. 2017; Kuncarayakti et al. 2018).

binary sensitivity remains but the ratio is now also metallicity dependent. Since the ratio is close to 1:1, small differences in the population ratio can be determined with relative ease – although the low number of objects in both classes still presents a problem. For comparison, we plot the ratio for M33 from Massey et al. (2016) and estimates for the SMC and LMC for which RSG data are drawn from Massey & Olsen (2003) and WR numbers from Neugent, Massey & Morrell (2018). As demonstrated by Dorn-Wallenstein & Levesque (2018), this line ratio is also dependent on the age of a simple stellar population, and so comparisons of Fig. 4 to data are not recommended for small starbursts or single-aged stellar clusters, but are likely to be robust in the larger populations such as galaxies that have been forming stars at a constant or slowly varying rate over 10^8 -yr timescales, such as M33.

3.1.2 Relative rates of SNe

While resolved stellar number counts such as those discussed above are promising binary fraction diagnostics, an alternative diagnostic can be derived from the manner in which these stars end their lives (e.g. Eldridge, Izzard & Tout 2008). Stars that have been stripped or gained mass through binary interactions may produce explosions which are classified differently, shifting between hydrogen-rich (SN II) and hydrogen-poor (SN I) classes. Amongst these transients, the ratio of stripped-envelope to hydrogen-rich core-collapse SNe shows promise as a diagnostic of binary fraction. As Fig. 5 demonstrates, this ratio declines with decreasing metallicity, tracking the fraction of stripped envelope massive stars in the population. As before, we overplot these models with a representative sample of observational data, showing both the vast range of estimates in the literature, and the large uncertainties on current measurements.

3.2 Cosmic evolution

The probes discussed above are sensitive to the massive star binary properties but relatively insensitive to the binary fraction amongst intermediate-mass and Solar-type stars. To probe these, we need to

identify sources or transients with low-mass progenitors, and take into account the longer evolutionary lifetime of these stars. Hence, we need to account for both a star formation and metallicity history over gigayear time-scales. This is challenging for any one galaxy, but plausible on a volume-averaged scale where extensive work has gone in to determining both the star formation rate (SFR) density evolution (Madau & Dickinson 2014) and the global metallicity evolution (Langer & Norman 2006).[1] In this context, we consider the cosmic evolution of SN rates, considering both core-collapse events (with massive progenitors) and thermonuclear detonations (with lower mass progenitors).

We adopt the same cosmic evolution prescription for SFR and Z as Eldridge et al. (2019) to calculate the SFR density distributed between different metallicities as a function of redshift. Using delay-time distributions and event rates from our models, we calculate the resultant cosmic evolution of SN rate per unit volume for each variant binary fraction distribution.[2] The results are shown in Fig. 6. The upper panel gives the evolution in the mean volumetric rate of each SN type between $z = 0$ and 6. In the lower panels, the evolution in the ratio of different types is shown out to $z = 2$ and compared to a compilation of observational data, as described below. We note that the lines indicating long gamma-ray bursts (LGRBs) include only the chemically homogeneous evolution pathway that dominates at the lowest metallicities, and neglects pathways that operate at higher metallicity (these may be included in later BPASS releases; see Chrimes et al. 2020).

To constrain the observed ratio of thermonuclear SN Ia rates to core-collapse SN rates, SN Ia (Melinder et al. 2012; Perrett et al. 2012; Graur et al. 2014; Okumura et al. 2014; Rodney et al. 2014; Cappellaro et al. 2015) and CCSN (Bazin et al. 2009; Melinder et al. 2012; Taylor et al. 2014; Petrushevska et al. 2016, and data compiled therein) volumetric rate data have been sorted into $\Delta z = 0.2$ bins, and where one or more rate estimates for both types exist in the same redshift bin, their ratio is taken. For the stripped-envelope SN fraction, we show the local rate ratio estimated from the LOSS survey (Shivvers et al. 2017) for galaxies at $z < 0.05$.

At low redshifts, a binary fraction close to unity is preferred for resolved studies of high-mass stars, with some indication that a high binary fraction is also preferred for Solar-type stars at very low metallicity (MS17; Moe et al. 2019). In each case, however, the observational uncertainties on current survey data are too large to distinguish between binary fractions with any degree of reliability, or to evaluate the redshift evolution of these rates.

As Fig. 6 demonstrates, the stripped-envelope fraction amongst core-collapse SNe evolves linearly with redshift, reflecting the slow evolution in the metallicity of the underlying stellar population. In contrast, the fraction of thermonuclear SNe Ia relative to core-collapse events remains near constant out to $z \sim 0.7$ before declining sharply. This results primarily from the much longer delay-time distribution of the SN Ia events. These require the evolution of relatively low-mass stars into white dwarfs, which then grow through binary interactions until the Chandrasekhar mass limit is reached.

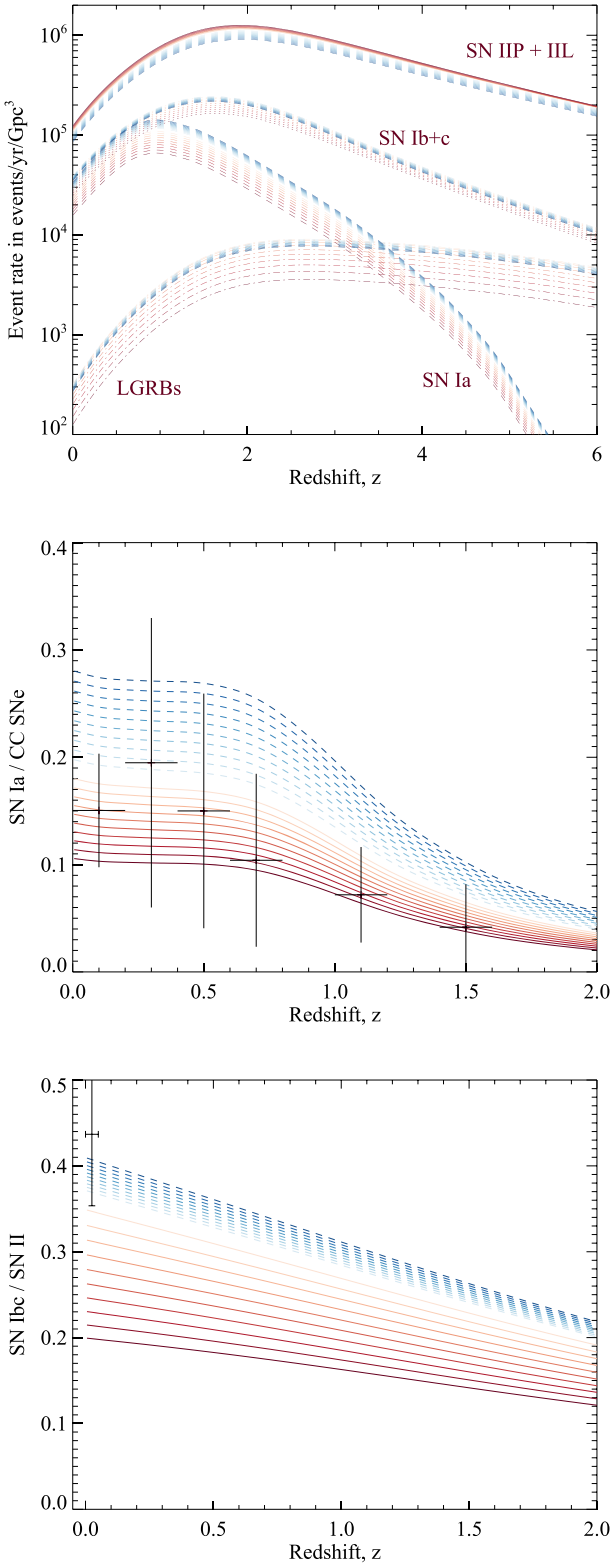

Figure 6. Cosmic evolution in volume-averaged SN rates by type and type ratios, as a function of binary fraction model, assuming the redshift evolution prescriptions for SFR and Z adopted in Eldridge et al. (2019). Overplotted points show the current state of observational constraints, compiled as described in Section 3.2.

[1]While other metallicity distribution estimates exist in the literature, the metallicity distribution of high-redshift star formation remains very uncertain, and we retain this prescription for comparison with earlier work. As Tang et al. (2020) explored, this prescription allows the correct recovery of local transient rates.

[2]We assume $\Omega_M = 0.286$, $\Omega_\Lambda = 0.714$, and $h = 0.696$.

4 DISCUSSION

As we have demonstrated, both the types of massive stars and their eventual SNe are sensitive to the presence of binary evolution pathways in the population. So are we approaching the point where resolved studies of massive stars may directly constrain the binary fraction of their underlying populations?

4.1 Observations of stellar-type ratios

The models presented in Section 3.1 are broadly consistent with the compilation of observational data shown, in terms of order of magnitude in number count ratios and underlying trends with metallicity. However, Figs 2–4 also demonstrate that there are large variations in observational estimates of stellar-type ratios. They also clearly indicate the very small number of measurements for which estimates of metallicity and massive star number count ratios are available. None the less, in certain ratios, and in particular the WR/RSG ratio, the uncertainties quoted on the data are already sufficiently small to interpret as binary fraction measurements. Given these factors, it is important to assess the robustness and appropriateness of the samples against which we are comparing.

In their recent comprehensive survey of resolved massive stars in M31 and M33, Massey et al. (2016) estimated that they were almost complete for WR stars but were incomplete for RSGs in M31 and had identified only a few per cent of the O stars present in the galaxies. In many of the observational samples reported, the completeness is still lower.

The O-star population is difficult to quantify due to confusion in star-forming regions and the typical brightness of individual stars. As a result, the number of O stars is often inferred from the ionizing photon flux inferred in a population, while the number and type of the WR stars is inferred from fitting of mass-scaled templates to diagnostic spectral features.[3] As a result, dusty stars may be undercounted, as may the hottest stars that radiate primarily in the ultraviolet. It is also an inconvenient fact that known WR stars have luminosities that scatter over two orders of magnitude (Crowther & Hadfield 2006) and so determining whether any individual ionized region has been irradiated by one star or many is challenging (see e.g. Rosslowe & Crowther 2015). This leads to a large scatter in the WR/O star number ratios reported, ranging from those that rely on clear identification of individual stars (incomplete) to those based entirely on inference from unresolved populations (heavily model and metallicity dependent). To illustrate the scale of these effects, in Fig. 2, we show two sets of points for the data of Miralles-Caballero et al. (2016): Open circles indicate the values given by the original authors as inferred from fitting unresolved stellar populations, and filled circles indicate values using the original WR numbers but modifying the inferred O-star count to account for the generally lower ionizing flux to O-star number ratio in the BPASS models. As the figure demonstrates, this increases the number of O stars inferred and brings this estimate closer into line with other estimates at similar metallicity. None the less, ratios inferred from this data set remain high compared to other data.

Each data set presents its own challenges to interpret. In several cases, no uncertainty is given on the published number ratios, and where possible this is inferred to give error bars on Fig. 2 from Poisson number count uncertainties on the inferred population. These have decreased with publication date as the number of detected sources per galaxy has risen. However, Poisson uncertainties do not account for systematic uncertainties in the underlying models used to infer the numbers, which can easily be of order a few tenths of a dex and thus span the model parameter space here. A fully consistent comparison between models and data would require the model completeness and calibration calculations to be undertaken using BPASS or a comparable code that incorporates binary evolution pathways.

Where WR stars are identified, either individually or through spectral fitting, they are typically classified into WC or WN types by the strength of carbon features in the spectrum. Thus, many of the uncertainties that affect the data in Fig. 2 also affect Fig. 3, with the added challenge that subdividing the small WR population adds to the Poisson uncertainties. Again, it is not always clear whether systematic modelling uncertainties are incorporated in the reported error bars for these data, and is likely that the true uncertainty on most of the data encompasses the full span of the models. In this context, it is interesting to note that above a metallicity of about half Solar, the data appear to favour models with low fractions of massive binaries, which are inconsistant with those observed in the local Universe (Sana et al. 2012, 2014; MS17). This may indicate that the number of WN stars in local galaxies is being underestimated using current template fitting techniques.

In comparison to the ratios discussed above, data for the WR/RSG ratio shown in Fig. 4 are very sparse in the literature: While RSG and WR populations have been studied separately in Local Group galaxies, it is rarely possible to evaluate whether the same regions have been surveyed in each case, the metallicity of the region being considered, and the relative levels of completeness in the samples. In the figure, we have shown estimates for the SMC and LMC for which RSG data are drawn from Massey & Olsen (2003) and WR numbers from Neugent et al. (2018). While these works originate from the same team, they are derived from very different imaging surveys, with different spatial coverage. As a result, the ratio can be compromised by the inclusion or omission of bright star-forming regions, or particularly young regions in one survey that may be omitted from the other, or conversely by a more extended, more mature stellar population. The third data point on Fig. 4 is that for M33 in which Massey et al. (2016) identified and spectroscopically confirmed 211 resolved WR stars and 220 RSGs and estimated that the survey was near complete for WR stars, and may also be complete for RSGs. This data point (at ∼0.5 Solar metallicity) is entirely consistent with the high binary fractions inferred for massive stars elsewhere in the local Universe. Unfortunately, the metallicity of this system is rather uncertain, with the 1σ error range admitting models with binary fractions of about 70 per cent or higher at $30\,M_{\odot}$. This point resulted from a substantial, multiyear campaign, but demonstrates the potential for constraints on the stellar binary fraction from large nearby galaxies.

In short, where data based on counting of individual stars are available (primarily in the SMC, LMC, and perhaps M33), the data may be used with caution. Where number counts are inferred from unresolved populations, stellar population model dependence and completeness must be carefully considered.

4.2 Constraints from star number counts

The extant observational data cannot distinguish between WR definitions in either the WR/O or the WR/RSG ratio, but hint that the revised luminosity limit suggested by Shenar et al. (2020) cannot reproduce the trend in WC/WN ratio with luminosity, for which our

[3]This approach is taken by all the data shown on Fig. 2, with individual WR stars only resolved in the very closest objects such as in parts of the LMC and SMC, and O-star numbers always derived indirectly.

original $\log(L/L_\odot) = 4.9$ luminosity limit, independent of metallicity, provides a good match. If there is indeed a strong metallicity dependence in the luminosity limit for WR spectroscopic identification, then the apparent discrepancy between the data and these predictions would suggest that the mass-loss rates, and especially their scaling with metallicity, in the BPASS stellar evolution models need to be revised. This question will be revisited in future work, since there is growing evidence that the mass-loss rates for WR stars and RSGs may need to be revised generally (e.g. Yoon 2015, 2017; Beasor et al. 2020; Neugent et al. 2020).

Setting aside the definition question, and focussing on our standard fixed-luminosity selection, the WR-to-O star ratio ranges from almost 8 per cent at a massive star binary fraction of unity to 6 per cent at a fraction of 40 per cent. As a result, distinguishing these populations at any reasonable degree of confidence would require an observed WR population well over 10 000 objects – far more than the total number of currently known WR stars in the Milky Way and its satellites. Thus, it is unlikely that this ratio will be determined to sufficient precision in any given galaxy to act as a strong constraint on the binary population.

Since binary processes are, at least in part, responsible for stripping the envelopes of stars that might otherwise evolve into WR stars, the WR/RSG ratio shows promise for evaluating the binary fraction in local galaxies in the near future. As Massey et al. (2016) demonstrated, this ratio can be determined in large nearby galaxies with a high degree of precision, given sufficient observational time and effort. The ratio is relatively insensitive to metallicity, mitigating an often-substantial degeneracy in the fitting of any data, and shows a strong sensitivity to the binary fraction in massive stars.

4.3 Future prospects for star count observations

Given the model dependence of indirectly inferred number counts, there is a clear preference for sensitive observations of resolved stars that allow counting of sources down to a luminosity limit of at least $\log(L/L_\odot) = 4.9$. In this context, it is worth considering what observations future instrumentation may enable in this area.

Science cases for the upcoming class of Extremely Large Telescopes (ELTs) include the detailed study of resolved stellar populations beyond the Local Group. The MICADO instrument on the European ELT,[4] for example, would expect to resolve and detect stars down to the horizontal branch at the distance of the Centaurus group (∼4.6 Mpc) in 5 h of integration, and so should produce complete catalogues for RSGs (Greggio et al. 2012). The fields of view expected for ELT instruments are expected to be less than 1 arcmin^2 (in some cases, significantly less) and, while this is suitable for mapping distant galaxies, will require large mosaics to map Local Group objects.

However, like many of the planned ELT instruments, MICADO is optimized to operate in the near-infrared, where adaptive optics can be most effectively deployed. As a result, it is unlikely to provide any information on WR and other luminous blue supergiant stars, for which near-ultraviolet imaging is preferred. Optical spectroscopy provides an alternate method for identifying WR stars, as described as above, but the first-light spectrograph on the ELT is not expected to be sufficiently blue-sensitive.

In the nearer term, resolved stellar populations may also be accessible to the *James Webb Space Telescope* (*JWST*) and an early release science programme in this area has been approved in Cycle 0 (Weisz et al. 2017). As is the case for the ELTs, *JWST* is a near-infrared optimized observatory with a small field of view. It will reach comparable sensitivities to the ELTs due to lying above the atmosphere, but suffers from a larger point spread function. As a result, confusion is likely to be an issue for observations at significant distances, while large mosaics will be necessary to map nearby galaxies. An optimal application for *JWST* may be study of individual star-forming regions or complexes, for which the metallicity, age, and binary fraction can be determined simultaneously, in contrast to the constant star formation case considered here.

The effort to identify and map WR stars, however, is unlikely to benefit significantly from either *JWST* or the ELTs due to their near-infrared optimization. For these, the current and ongoing effort to identify these sources from integral field spectroscopy and optical photometry is unlikely to be improved upon before the construction of a blue-sensitive, large aperture observatory such as the proposed LUVOIR.[5] Continuing this work, with a goal of highly complete spectroscopic follow-up, wherever possible of individually resolved sources, is essential if constraints on the binary fraction are to be obtained from stellar-type number count ratios.

It should also be noted that while these instruments are not optimized for mapping the large angular scales subtended by Local Group galaxies, analysis of the resolved stellar populations in more compact and distant objects may allow average ratios may be derived for larger samples of galaxies as a function of metallicity, which will shed light on these populations. As with any observation, it will be crucial to map different stellar populations, fit any spectra and determine metallicities self-consistently and for stars drawn from the same spatial regions, before comparison can be made to model predictions such as those presented here.

4.4 Constraints from SN observations

All the number count ratios involving WR stars are, however, relatively insensitive to the binary fraction in low-mass binary stars in the population, as might be expected. The strongest diagnostic of low-mass binaries studied here is the ratio of SN Ia to core-collapse SNe. As Fig. 6 demonstrates, distinguishing between high-mass star binary fractions requires precision on the SN Ia or SN Ibc fraction of about 1 per cent at $z = 0$ and becomes progressively more difficult at higher redshifts. A similar precision is needed to constrain binary fraction as a function of metallicity, as seen in Fig. 5 in which the data uncertainties are dominated by corrections for completeness in calibration or follow-up. Since stripped-envelope SNe are often harder to classify from light curves than hydrogen-rich SN II, many of the estimates shown are likely to be lower limits.

While demanding, the required precision promises to be eminently achievable with the upcoming Legacy Survey of Space and Time (LSST) at the Vera Rubin Observatory. LSST will carry out a deep, high-cadence survey of the transient sky, expecting to find of the order of 10^5 SNe Ia per year, and a comparable number of core-collapse events (LSST Science Collaboration 2009; see chapter 11). The majority of these will lie in the range $z = 0.2$–1, an interval over which the ratio of event type is expected to change significantly – as Fig. 6 shows. Given the expected rate of events, if all could be accurately typed, measurements would be possible of the SN-type ratios in 10 redshift bins at about 1 per cent precision – sufficient to distinguish between high and low binary fractions at both ends of the mass function. With lower numbers, of only about 1000 SNe per

[4]EELT; available at https://www.eso.org/sci/facilities/eelt/.

[5]https://asd.gsfc.nasa.gov/luvoir/.

$\Delta z = 0.1$ bin, the number of measured SNe Ia is expected to be 200, SNe Ibc about 240, and SN II about 560, giving 7, 6, and 4 per cent uncertainty, respectively, on measured rates from simple Poisson statistic arguments – these then need to be corrected for observational biases. With 10 000 SNe per bin, the Poisson uncertainties drop to 2, 2, and 1 per cent, sufficient to identify the binary fraction to within ± 1 model on our current grid. This will be true for CCSN out to $z = 0.5$ in 1 yr (Lien & Fields 2009). Higher redshifts may be accessible through wider redshift bins, while extended data as the survey continues will enable narrower bins to be used, probing more details such as the metallicity history of the galaxy evolution.

We note that this assumes redshift uncertainties are smaller than the bin size. At this redshift range, this should be possible in the majority of host galaxies through photometric redshift determination. It also assumes that SNe can be accurately typed by their light curves in the absence of large-scale spectroscopy (expected to be true; LSST Science Collaboration 2009).

We have also assumed that the same binary fraction applies at all metallicities, and that the same distribution of period and mass ratio applies at all binary fractions. These are more difficult to quantify or justify as assumptions and further studies with a more extensive suite of models will be required to evaluate the extent to which the joint posterior probability distribution of these parameters can be determined. Intriguingly, the wide area and deep limits of the LSST data will enable lensed SNe to be observed at much higher redshifts. Rydberg et al. (2020) estimated that up to 120 lensed SNe at $z \sim 5$–7 could be detected by the LSST Wide Deep Fast survey, with more sources at intermediate redshift. While the precision in any type ratio derived from this higher redshift population would necessarily be large, it will provide an important test of the metallicity distribution assumed for high-redshift star formation in this model.

In very local examples, identified in LSST or other survey data on well-studied local galaxies, it might be possible to determine both the SN-type ratio and WR/RSG ratio, at least for large galaxies. A simultaneous analysis of the SN-type ratios and WR/RSG ratios for the same sample of galaxies would be a powerful diagnostic tool. This combination yields a diagnostic grid in binary fraction versus metallicity for $Z > 0.002$. Again, a precision of about 1 per cent is required to distinguish between models in SN-type ratio, while a lower precision (about 10 per cent) is sufficient in the harder-to-measure stellar-type ratio, and this is still likely to be challenging for the current and next generation of facilities.

5 CONCLUSIONS

Analysis of the type statistics of massive stars has the potential to constrain the fraction of binary stars in stellar populations. However, the degree of precision required is significantly higher than that obtained by current surveys.

Adopting the metallicity dependence suggested by Shenar et al. (2020) for the minimum luminosity of classical WR stars significantly changes both the metallicity and binary fraction dependence of WR number-type ratios. Both the WR/O and WR/RSG ratios become more strongly metallicity dependent, while the WC/WN ratio becomes less so, in mild conflict with recent observational evidence. More data on these line ratios (drawn from large, complete sample of resolved stars, or potentially from the integrated light of well-aged stellar clusters) are needed before the new WR definition is adopted. We note that Shenar et al. do not argue that stripped helium stars at luminosities between $\log(L/L_{\odot}) = 4.9$ and their metallicity-dependent limit do not exist or do not affect their surroundings, but rather than they would not show the characteristic spectral features indicative of strong stellar winds.

The synergy between the capabilities of upcoming telescopes in the fields of resolved stellar populations (e.g. *JWST*, ELTs) and SN rates (e.g. LSST) has the capacity to constrain the binary fraction as a function of metallicity and even redshift. LSST's vast data set will likely allow both the high- and low-mass binary fractions to be determined to a high degree of precision, with some constraints on its metallicity evolution if the cosmic evolution of SN-type ratios can be measured with sufficient precision. This relies on reliable typing of SNe, either photometrically or spectroscopically.

We have focused here on the effect of varying the total binary fraction at a given mass. Since stars in wide binaries (log(initial period/days) > 4) are unlikely to interact in a Hubble time, and are treated as single stars in BPASS, this variation is degenerate with fixing the binary fraction, but instead biasing its period distribution towards closer binaries. Distinguishing between these scenarios is likely to be far harder, in the absence of spectroscopic period determinations for large numbers of distant stellar populations – beyond the capabilities of even planned telescopes. Constraining the period and mass ratio distributions based on very local stars is likely to remain necessary for some time to come.

ACKNOWLEDGEMENTS

ERS received support from United Kingdom Science and Technology Facilities Council (STFC) grant number ST/P000495/1 and ST/T000406/1. AAC was supported by STFC studentship 1763016. JJE acknowledges support from the University of Auckland and the Royal Society Te Apārangi of New Zealand under the Marsden Fund. BPASS would not be possible without the computational resources of the University of Auckland's NZ eScience Infrastructure (NeSI) Pan Cluster and the University of Warwick's Scientific Computing Research Technology Platform (SCRTP).

DATA AVAILABILITY

The model data reported here is tabulated in the appendix and will be made available via the BPASS websites – bpass.auckland.ac.uk or warwick.ac.uk/bpass.

REFERENCES

Bazin G. et al., 2009, A&A, 499, 653
Beasor E. R., Davies B., Smith N., van Loon J. T., Gehrz R. D., Figer D. F., 2020, MNRAS, 492, 5994
Bibby J. L., Crowther P. A., 2012, MNRAS, 420, 3091
Boissier S., Prantzos N., 2009, A&A, 503, 137
Bruzual G., Charlot S., 2003, MNRAS, 344, 1000
Cappellaro E. et al., 2015, A&A, 584, A62
Chrimes A. A., Stanway E. R., Eldridge J. J., 2020, MNRAS, 491, 3479
Crowther P. A., Hadfield L. J., 2006, A&A, 449, 711
Crowther P. A., Carpano S., Hadfield L. J., Pollock A. M. T., 2007, A&A, 469, L31
De Donder E., Vanbeveren D., 1998, A&A, 333, 557
Dorn-Wallenstein T. Z., Levesque E. M., 2018, ApJ, 867, 125
Dorn-Wallenstein T. Z., Levesque E. M., 2020, ApJ, 896, 164
Eldridge J. J., Stanway E. R., 2009, MNRAS, 400, 1019
Eldridge J. J., Stanway E. R., 2012, MNRAS, 419, 479
Eldridge J. J., Stanway E. R., 2016, MNRAS, 462, 3302
Eldridge J. J., Izzard R. G., Tout C. A., 2008, MNRAS, 384, 1109
Eldridge J. J., Stanway E. R., Xiao L., McClelland L. A. S., Taylor G., Ng M., Greis S. M. L., Bray J. C., 2017, Publ. Astron. Soc. Aust., 34, e058 (E17)

Eldridge J. J., Xiao L., Stanway E. R., Rodrigues N., Guo N. Y., 2018, Publ. Astron. Soc. Aust., 35, 49
Eldridge J. J., Stanway E. R., Tang P. N., 2019, MNRAS, 482, 870
Götberg Y., de Mink S. E., McQuinn M., Zapartas E., Groh J. H., Norman C., 2020, A&A, 634, A134
Graur O. et al., 2014, ApJ, 783, 28
Graur O., Bianco F. B., Huang S., Modjaz M., Shivvers I., Filippenko A. V., Li W., Eldridge J. J., 2017, ApJ, 837, 120
Greggio L., Falomo R., Zaggia S., Fantinel D., Uslenghi M., 2012, PASP, 124, 653
Hadfield L. J., Crowther P. A., 2007, MNRAS, 381, 418
Kelly P. L., Kirshner R. P., 2012, ApJ, 759, 107
Kuncarayakti H. et al., 2018, A&A, 613, A35
Langer N., Norman C. A., 2006, ApJ, 638, L63
Le Borgne D., Rocca-Volmerange B., Prugniel P., Lançon A., Fioc M., Soubiran C., 2004, A&A, 425, 881
Lien A., Fields B. D., 2009, J. Cosmol. Astropart. Phys., 2009, 047
LSST Science Collaboration, 2009, preprint (arXiv:0912.0201)
Ma X., Hopkins P. F., Kasen D., Quataert E., Faucher-Giguère C.-A., Kereš D., Murray N., Strom A., 2016, MNRAS, 459, 3614
Madau P., Dickinson M., 2014, ARA&A, 52, 415
Maeder A., Meynet G., 1994, A&A, 287, 803
Maeder A., Lequeux J., Azzopardi M., 1980, A&A, 90, L17
Maraston C., 2005, MNRAS, 362, 799
Massey P., Olsen K. A. G., 2003, AJ, 126, 2867
Massey P., Neugent K. F., Smart B. M., 2016, AJ, 152, 62
Melinder J. et al., 2012, A&A, 545, A96
Miralles-Caballero D. et al., 2016, A&A, 592, A105
Moe M., Di Stefano R., 2017, ApJS, 230, 15 (MS17)
Moe M., Kratter K. M., Badenes C., 2019, ApJ, 875, 61
Monreal-Ibero A., Walsh J. R., Iglesias-Páramo J., Sandin C., Relaño M., Pérez-Montero E., Vílchez J., 2017, A&A, 603, A130
Neugent K., Massey P., 2019, Galaxies, 7, 74
Neugent K. F., Massey P., Morrell N., 2018, ApJ, 863, 181
Neugent K. F., Massey P., Georgy C., Drout M. R., Mommert M., Levesque E. M., Meynet G., Ekström S., 2020, ApJ, 889, 44
Okumura J. E. et al., 2014, PASJ, 66, 49
Perrett K. et al., 2012, AJ, 144, 59
Petrushevska T. et al., 2016, A&A, 594, A54
Prieto J. L., Stanek K. Z., Beacom J. F., 2008, ApJ, 673, 999
Rodney S. A. et al., 2014, AJ, 148, 13
Rosslowe C. K., Crowther P. A., 2015, MNRAS, 447, 2322
Rydberg C.-E., Whalen D. J., Maturi M., Collett T., Carrasco M., Magg M., Klessen R. S., 2020, MNRAS, 491, 2447
Sana H. et al., 2012, Science, 337, 444
Sana H. et al., 2013, A&A, 550, A107
Sana H. et al., 2014, ApJS, 215, 15
Shenar T., Gilkis A., Vink J. S., Sana H., Sand er A. A. C., 2020, A&A, 634, A79
Shivvers I. et al., 2017, PASP, 129, 054201
Stanway E. R., Eldridge J. J., 2018, MNRAS, 479, 75
Stanway E. R., Eldridge J. J., 2019, A&A, 621, A105
Stanway E. R., Eldridge J. J., Greis S. M. L., Davies L. J. M., Wilkins S. M., Bremer M. N., 2014, MNRAS, 444, 3466
Stanway E. R., Eldridge J. J., Becker G. D., 2016, MNRAS, 456, 485
Stanway E. R., Chrimes A. A., Eldridge J. J., Stevance H. F., 2020, MNRAS, 495, 4605 (S20)
Steidel C. C., Strom A. L., Pettini M., Rudie G. C., Reddy N. A., Trainor R. F., 2016, ApJ, 826, 159
Steidel C. C., Bogosavljević M., Shapley A. E., Reddy N. A., Rudie G. C., Pettini M., Trainor R. F., Strom A. L., 2018, ApJ, 869, 123
Tang P. N., Eldridge J. J., Stanway E. R., Bray J. C., 2020, MNRAS, 493, L6
Taylor M. et al., 2014, ApJ, 792, 135
Tinsley B. M., Gunn J. E., 1976, ApJ, 203, 52
Traven G. et al., 2020, A&A, 638, A145
Tutukov A. V., Yungelson L. R., Iben, Icko J., 1992, ApJ, 386, 197
Vanbeveren D., De Donder E., Van Bever J., Van Rensbergen W., De Loore C., 1998, New Astron., 3, 443
Vrancken M., De Greve J. P., Yungelson L., Tutukov A., 1991, A&A, 249, 411
Weisz D. R. et al., 2017, The Resolved Stellar Populations Early Release Science Program, JWST Proposal ID 1334, Cycle 0 Early Release Science
Wilkins S. M., Feng Y., Di-Matteo T., Croft R., Stanway E. R., Bouwens R. J., Thomas P., 2016, MNRAS, 458, L6
Xiao L., Eldridge J. J., 2015, MNRAS, 452, 2597
Xiao L., Stanway E. R., Eldridge J. J., 2018, MNRAS, 477, 904
Yoon S.-C., 2015, Publ. Astron. Soc. Aust., 32, e015
Yoon S.-C., 2017, MNRAS, 470, 3970
Zapartas E., de Mink S. E., Justham S., Smith N., Renzo M., de Koter A., 2020, preprint (arXiv:2002.07230)
Zhang F., Li L., Kang X., Zhuang Y., Han Z., 2013, MNRAS, 433, 1039

APPENDIX A: BINARY FRACTION DISTRIBUTIONS

The binary fraction, $f_{\rm bin}$, in these models is defined as a function of mass by a parametrization:

$$f_{\rm bin}(M_i) = \min([1.0,\ A \times \log_{10}(M_i) + f_{\rm bin}(1\,{\rm M}_\odot)]),$$

where M_i is the initial mass of the primary or single star in Solar masses and A is a constant selected to produce the two model sets shown in Fig. 1. Values of A, and $f_{\rm bin}(1\,{\rm M}_\odot)$ used here are given in Table A1, together with resultant values for $f_{\rm bin}(30\,{\rm M}_\odot)$.

We also provide numerical values for the set 2 (massive star binary fraction) models in Figs 2–5 in Tables A2–A4.

Table A1. Parameters of the binary fraction functions used in this work.

Set	Model	A	$f_{\rm bin}(1\,{\rm M}_\odot)$	$f_{\rm bin}(30\,{\rm M}_\odot)$
1	0	0.399	0.442	1.000
	1	0.354	0.504	1.000
	2	0.310	0.566	1.000
	3	0.266	0.628	1.000
	4	0.222	0.690	1.000
	5	0.177	0.752	1.000
	6	0.133	0.814	1.000
	7	0.089	0.876	1.000
	8	0.044	0.938	1.000
	9	0.000	1.000	1.000
2	0	0.399	0.380	0.969
	1	0.354	0.380	0.903
	2	0.310	0.380	0.838
	3	0.266	0.380	0.772
	4	0.222	0.380	0.707
	5	0.177	0.380	0.641
	6	0.133	0.380	0.576
	7	0.089	0.380	0.510
	8	0.044	0.380	0.445
	9	0.000	0.380	0.380

Table A2. Predicted number count ratios for model set 2, assuming 100 Myr of constant star formation at 1 $M_\odot$ yr^{-1}.

	$\log(L^{WR}/L_\odot) > 4.9$)				$\log(L^{WR}/L_\odot) > 4.9 - \log(Z/0.014)$		
$Z = 0.001$ model	N(WR/O)	N(WC/WN)	N(WR/RSG)	N(SN Ibc/SN II)	N(WR/O)	N(WC/WN)	N(WR/RSG)
0	0.012 66	0.112 28	1.439 95	0.033 82	0.001 64	0.282 43	0.186 95
1	0.012 24	0.115 46	1.295 43	0.032 80	0.001 66	0.282 77	0.175 94
2	0.011 69	0.118 15	1.153 10	0.031 55	0.001 66	0.286 57	0.163 94
3	0.011 05	0.119 58	1.018 33	0.030 23	0.001 63	0.293 47	0.149 88
4	0.010 37	0.120 02	0.893 45	0.028 82	0.001 57	0.296 75	0.135 33
5	0.009 66	0.120 50	0.779 81	0.027 40	0.001 51	0.300 30	0.122 08
6	0.008 92	0.121 09	0.676 02	0.025 98	0.001 45	0.304 32	0.109 98
7	0.008 15	0.121 82	0.580 83	0.024 56	0.001 39	0.308 89	0.098 87
8	0.007 36	0.122 74	0.493 22	0.023 15	0.001 32	0.314 16	0.088 66
9	0.006 52	0.123 93	0.412 33	0.021 73	0.001 25	0.320 28	0.079 22
$Z = 0.002$ model	N(WR/O)	N(WC/WN)	N(WR/RSG)	N(SN Ibc/SN II)	N(WR/O)	N(WC/WN)	N(WR/RSG)
0	0.018 64	0.135 97	1.081 92	0.060 36	0.004 63	0.409 66	0.268 68
1	0.017 99	0.140 53	0.980 22	0.058 66	0.004 65	0.412 91	0.253 10
2	0.017 19	0.144 80	0.879 88	0.056 53	0.004 58	0.421 17	0.234 61
3	0.016 28	0.146 93	0.784 40	0.054 07	0.004 45	0.423 33	0.214 18
4	0.015 31	0.147 63	0.694 55	0.051 31	0.004 26	0.420 72	0.193 21
5	0.014 29	0.148 43	0.611 90	0.048 55	0.004 06	0.417 72	0.173 90
6	0.013 25	0.149 40	0.535 65	0.045 82	0.003 86	0.414 30	0.156 09
7	0.012 16	0.150 58	0.465 09	0.043 10	0.003 65	0.410 38	0.139 61
8	0.011 04	0.152 04	0.399 61	0.040 40	0.003 43	0.405 84	0.124 32
9	0.009 87	0.153 93	0.338 67	0.037 71	0.003 21	0.400 52	0.110 08
$Z = 0.003$ model	N(WR/O)	N(WC/WN)	N(WR/RSG)	N(SN Ibc/SN II)	N(WR/O)	N(WC/WN)	N(WR/RSG)
0	0.024 38	0.149 22	0.867 75	0.079 49	0.008 11	0.448 29	0.288 64
1	0.023 55	0.155 02	0.790 20	0.077 14	0.008 09	0.455 52	0.271 41
2	0.022 59	0.160 60	0.715 24	0.074 83	0.007 99	0.463 16	0.253 02
3	0.021 51	0.164 17	0.643 10	0.072 35	0.007 79	0.465 16	0.233 01
4	0.020 34	0.166 40	0.574 26	0.069 47	0.007 52	0.463 20	0.212 42
5	0.019 12	0.168 98	0.510 53	0.066 60	0.007 24	0.460 98	0.193 34
6	0.017 85	0.172 05	0.451 37	0.063 74	0.006 95	0.458 49	0.175 64
7	0.016 54	0.175 75	0.396 32	0.060 90	0.006 64	0.455 68	0.159 16
8	0.015 18	0.180 30	0.344 96	0.058 07	0.006 33	0.452 50	0.143 78
9	0.013 76	0.186 02	0.296 93	0.055 26	0.006 00	0.448 86	0.129 41
$Z = 0.004$ model	N(WR/O)	N(WC/WN)	N(WR/RSG)	N(SN Ibc/SN II)	N(WR/O)	N(WC/WN)	N(WR/RSG)
0	0.033 03	0.157 39	0.903 29	0.109 90	0.013 75	0.416 44	0.376 12
1	0.031 86	0.163 85	0.826 59	0.106 21	0.013 59	0.425 44	0.352 66
2	0.030 55	0.169 82	0.752 35	0.102 68	0.013 33	0.433 43	0.328 17
3	0.029 10	0.174 22	0.680 42	0.099 18	0.012 93	0.438 04	0.302 27
4	0.027 54	0.177 44	0.611 43	0.095 44	0.012 44	0.439 63	0.276 07
5	0.025 93	0.181 19	0.547 11	0.091 74	0.011 92	0.441 37	0.251 63
6	0.024 26	0.185 61	0.487 01	0.088 09	0.011 40	0.443 35	0.228 80
7	0.022 53	0.190 91	0.430 74	0.084 48	0.010 85	0.445 60	0.207 42
8	0.020 75	0.197 39	0.377 93	0.080 91	0.010 29	0.448 19	0.187 36
9	0.018 91	0.205 48	0.328 28	0.077 38	0.009 70	0.451 19	0.168 49

Note. Metallicities shown are $Z = 0.001$, 0.002, 0.003, and 0.004.

Table A3. Predicted number count ratios for model set 2, assuming 100 Myr of constant star formation at $1\,M_{\odot}\,yr^{-1}$.

	$\log(L^{WR}/L_{\odot}) > 4.9$)				$\log(L^{WR}/L_{\odot}) > 4.9 - \log(Z/0.014)$		
$Z = 0.006$ model	N(WR/O)	N(WC/WN)	N(WR/RSG)	N(SN Ibc/SN II)	N(WR/O)	N(WC/WN)	N(WR/RSG)
0	0.036 69	0.207 63	0.880 75	0.122 37	0.021 68	0.410 32	0.520 48
1	0.035 57	0.216 17	0.810 00	0.118 05	0.021 35	0.420 72	0.486 19
2	0.034 31	0.224 66	0.741 95	0.114 57	0.020 91	0.430 80	0.452 06
3	0.032 92	0.231 88	0.676 12	0.111 44	0.020 33	0.438 52	0.417 48
4	0.031 44	0.238 65	0.613 62	0.108 34	0.019 67	0.444 92	0.383 95
5	0.029 91	0.246 43	0.555 26	0.105 31	0.018 99	0.452 05	0.352 62
6	0.028 32	0.255 47	0.500 63	0.102 34	0.018 29	0.460 06	0.323 30
7	0.026 68	0.266 12	0.449 39	0.099 43	0.017 56	0.469 12	0.295 81
8	0.024 99	0.278 85	0.401 24	0.096 57	0.016 81	0.479 45	0.269 96
9	0.023 23	0.294 31	0.355 90	0.093 77	0.016 03	0.491 35	0.245 63
$Z = 0.008$ model	N(WR/O)	N(WC/WN)	N(WR/RSG)	N(SN Ibc/SN II)	N(WR/O)	N(WC/WN)	N(WR/RSG)
0	0.044 44	0.279 50	0.923 04	0.192 84	0.031 73	0.440 81	0.659 04
1	0.043 15	0.290 24	0.853 37	0.184 38	0.031 12	0.453 37	0.615 38
2	0.041 73	0.301 30	0.786 27	0.176 26	0.030 39	0.466 19	0.572 56
3	0.040 13	0.311 17	0.720 33	0.168 31	0.029 48	0.477 28	0.529 12
4	0.038 39	0.320 33	0.656 68	0.160 39	0.028 44	0.487 02	0.486 45
5	0.036 59	0.330 85	0.596 93	0.152 62	0.027 36	0.498 00	0.446 38
6	0.034 73	0.343 07	0.540 74	0.145 00	0.026 25	0.510 48	0.408 71
7	0.032 80	0.357 45	0.487 81	0.137 52	0.025 10	0.524 80	0.373 22
8	0.030 82	0.374 59	0.437 86	0.130 18	0.023 91	0.541 39	0.339 72
9	0.028 76	0.395 39	0.390 65	0.122 96	0.022 68	0.560 84	0.308 06
$Z = 0.010$ model	N(WR/O)	N(WC/WN)	N(WR/RSG)	N(SN Ibc/SN II)	N(WR/O)	N(WC/WN)	N(WR/RSG)
0	0.053 48	0.358 72	0.937 47	0.260 18	0.044 50	0.464 73	0.780 08
1	0.051 86	0.371 54	0.871 10	0.248 13	0.043 40	0.478 69	0.728 93
2	0.050 13	0.384 56	0.807 18	0.236 51	0.042 18	0.492 73	0.679 20
3	0.048 20	0.396 54	0.743 93	0.224 87	0.040 77	0.505 42	0.629 17
4	0.046 17	0.408 34	0.683 10	0.213 09	0.039 25	0.517 56	0.580 74
5	0.044 08	0.421 79	0.625 78	0.201 46	0.037 69	0.531 25	0.535 09
6	0.041 94	0.437 27	0.571 67	0.189 97	0.036 09	0.546 79	0.492 00
7	0.039 75	0.455 29	0.520 51	0.178 62	0.034 46	0.564 60	0.451 26
8	0.037 50	0.476 51	0.472 07	0.167 41	0.032 78	0.585 20	0.412 68
9	0.035 19	0.501 88	0.426 13	0.156 34	0.031 06	0.609 30	0.376 10
$Z = 0.014$ model	N(WR/O)	N(WC/WN)	N(WR/RSG)	N(SN Ibc/SN II)	N(WR/O)	N(WC/WN)	N(WR/RSG)
0	0.066 76	0.542 51	1.141 12	0.510 89	0.066 76	0.542 51	1.141 12
1	0.064 96	0.555 93	1.065 99	0.483 15	0.064 96	0.555 93	1.065 99
2	0.063 06	0.568 58	0.994 68	0.456 31	0.063 06	0.568 58	0.994 68
3	0.060 90	0.580 21	0.922 96	0.428 48	0.060 90	0.580 21	0.922 96
4	0.058 49	0.592 79	0.851 84	0.400 73	0.058 49	0.592 79	0.851 84
5	0.056 01	0.607 03	0.784 50	0.373 79	0.056 01	0.607 03	0.784 50
6	0.053 48	0.623 30	0.720 68	0.347 63	0.053 48	0.623 30	0.720 68
7	0.050 88	0.642 05	0.660 11	0.322 22	0.050 88	0.642 05	0.660 11
8	0.048 22	0.663 90	0.602 54	0.297 52	0.048 22	0.663 90	0.602 54
9	0.045 49	0.689 68	0.547 75	0.273 50	0.045 49	0.689 68	0.547 75

Note. Metallicities shown are $Z = 0.006$, 0.008, 0.010, and 0.014.

Table A4. Predicted number count ratios for model set 2, assuming 100 Myr of constant star formation at 1 $M_\odot$ yr^{-1}.

	$\log(L^{WR}/L_\odot) > 4.9$)				$\log(L^{WR}/L_\odot) > 4.9 - \log(Z/0.014)$		
$Z = 0.020$ model	N(WR/O)	N(WC/WN)	N(WR/RSG)	N(SN Ibc/SN II)	N(WR/O)	N(WC/WN)	N(WR/RSG)
0	0.077 66	0.511 62	1.256 68	0.520 02	0.077 66	0.511 62	1.256 68
1	0.076 11	0.524 35	1.177 84	0.492 06	0.076 11	0.524 35	1.177 84
2	0.074 45	0.538 31	1.103 41	0.466 75	0.074 45	0.538 31	1.103 41
3	0.072 43	0.552 82	1.028 03	0.442 28	0.072 43	0.552 82	1.028 03
4	0.070 19	0.567 97	0.954 21	0.418 68	0.070 19	0.567 97	0.954 21
5	0.067 88	0.585 00	0.884 30	0.395 78	0.067 88	0.585 00	0.884 30
6	0.065 50	0.604 26	0.818 02	0.373 56	0.065 50	0.604 26	0.818 02
7	0.063 04	0.626 24	0.755 09	0.351 99	0.063 04	0.626 24	0.755 09
8	0.060 49	0.651 54	0.695 26	0.331 04	0.060 49	0.651 54	0.695 26
9	0.057 87	0.680 99	0.638 32	0.310 68	0.057 87	0.680 99	0.638 32
$Z = 0.030$ model	N(WR/O)	N(WC/WN)	N(WR/RSG)	N(SN Ibc/SN II)	N(WR/O)	N(WC/WN)	N(WR/RSG)
0	0.110 31	0.595 39	1.463 30	0.555 40	0.110 31	0.595 39	1.463 30
1	0.108 20	0.606 31	1.379 30	0.513 66	0.108 20	0.606 31	1.379 30
2	0.105 98	0.617 99	1.301 48	0.474 14	0.105 98	0.617 99	1.301 48
3	0.103 22	0.631 05	1.221 40	0.435 95	0.103 22	0.631 05	1.221 40
4	0.100 13	0.644 81	1.141 76	0.399 16	0.100 13	0.644 81	1.141 76
5	0.096 97	0.660 07	1.066 03	0.363 75	0.096 97	0.660 07	1.066 03
6	0.093 74	0.677 07	0.993 95	0.329 61	0.093 74	0.677 07	0.993 95
7	0.090 43	0.696 15	0.925 27	0.296 70	0.090 43	0.696 15	0.925 27
8	0.087 04	0.717 70	0.859 74	0.264 94	0.087 04	0.717 70	0.859 74
9	0.083 56	0.742 24	0.797 16	0.234 27	0.083 56	0.742 24	0.797 16
$Z = 0.040$ model	N(WR/O)	N(WC/WN)	N(WR/RSG)	N(SN Ibc/SN II)	N(WR/O)	N(WC/WN)	N(WR/RSG)
0	0.150 25	0.556 61	1.842 68	0.650 91	0.150 25	0.556 61	1.842 68
1	0.14754	0.563 65	1.739 27	0.605 91	0.147 54	0.563 65	1.739 27
2	0.144 57	0.572 26	1.642 98	0.561 32	0.144 57	0.572 26	1.642 98
3	0.140 84	0.582 34	1.543 63	0.516 76	0.140 84	0.582 34	1.543 63
4	0.136 66	0.593 23	1.444 49	0.473 17	0.136 66	0.593 23	1.444 49
5	0.132 38	0.605 25	1.350 24	0.431 03	0.132 38	0.605 25	1.350 24
6	0.128 01	0.618 57	1.260 54	0.390 30	0.128 01	0.618 57	1.260 54
7	0.123 55	0.633 40	1.175 07	0.350 88	0.123 55	0.633 40	1.175 07
8	0.118 99	0.650 03	1.093 54	0.312 73	0.118 99	0.650 03	1.093 54
9	0.114 33	0.668 79	1.015 69	0.275 78	0.114 33	0.668 79	1.015 69

Notes. Metallicities shown are $Z = 0.020$, 0.030, and 0.040. In this range, the new WR definition does not affect the number-type ratios.

This paper has been typeset from a TEX/LATEX file prepared by the author.